Macrophage ontogeny underlies differences in tumor-specific education in brain malignancies

Robert L. Bowman[1,2], Florian Klemm[1,3,4], Leila Akkari[1,3,4], Stephanie M. Pyonteck[1], Lisa Sevenich[1], Daniela F. Quail[1], Surajit Dhara[5], Kenishana Simpson[1], Eric E. Gardner[6], Christine A. Iacobuzio-Donahue[5,7], Cameron W. Brennan[8], Viviane Tabar[8], Philip H. Gutin[8], and Johanna A. Joyce[1,3,4,#]

[#] Correspondence to: johanna@joycelab.org

Supplemental Figure 1: Genetic lineage tracing models provide high fidelity approaches for isolating TAM BMDM and TAM MG. Related to Figure 1.

Supplemental Figure 2: TAM BMDM and TAM MG possess model and cell type specific gene expression patterns associated with baseline chromatin states. Related to Figure 2.

Supplemental Figure 3: TAM BMDM and TAM MG possess differential open chromatin in cell-type specific genes. Related to Figure 3.

Supplemental Figure 4: Cd49d and Cd11a are enriched in TAM BMDM compared to TAM MG in multiple mouse models of brain malignancy. Related to Figure 4.

Supplemental Figure 5: *ITGA4* and markers of TAM BMDM are present in purified cell types and in whole tumor expression data from patients. Related to Figure 5.

SUPPLEMENTAL TABLES

Supplemental Table S1A and S1B: Conserved and specific genes upregulated in TAM populations compared to normal microglia and monocytes. Related to Figure 1I.

Supplemental Table S2: Differentially expressed genes between TAM BMDM and TAM MG in both GEMM and GL261 models. Related to Figure 2A.

Supplemental Table S3: Differentially expressed genes between GEMM and GL261 models for both TAM BMDM and TAM MG. Related to Figure 2A and Figure S2C.

Supplemental Table S4: Lists of cell type-specific and TAM education-specific gene sets for TAM BMDM and TAM MG. Related to Figure 2E and Figure S2D.

Supplemental Table S5A, S5B and S5C: Differentially enriched ATAC-Seq peaks, motif scores, and transcription factor activities between TAM BMDM and TAM MG. Related to Figure 3.

SUPPLEMENTAL EXPERIMENTAL PROCEDURES

Bowman et al, Figure S1

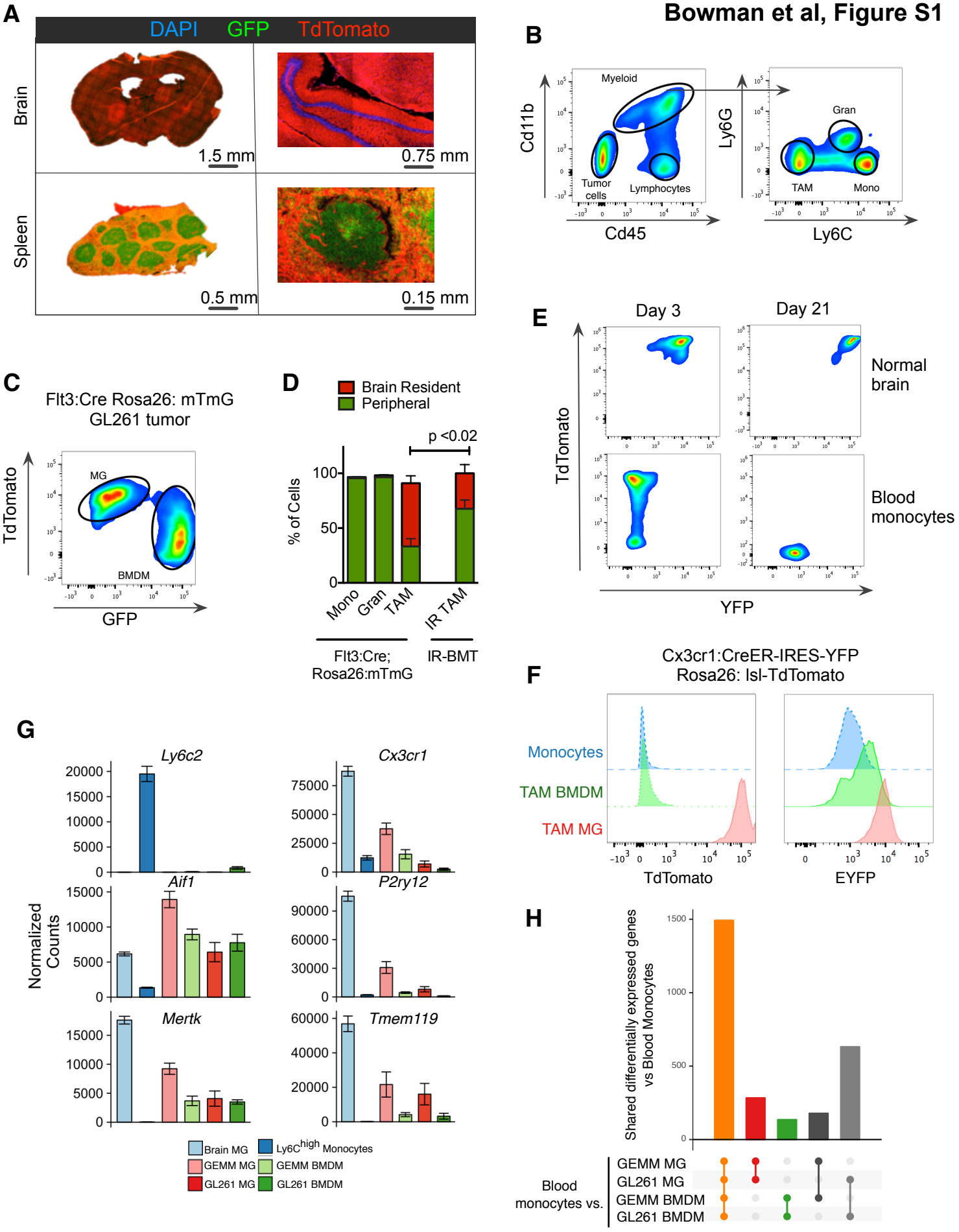

Supplemental Figure 1: Genetic lineage tracing models provide high fidelity approaches for isolating TAM BMDM and TAM MG. Related to Figure 1.

(A) Representative tiled immunofluorescence image of brain (top) and spleen (bottom) in a Flt:Cre Rosa26:mTmG mouse. TdTomato is indicated in red, GFP in green, and DAPI in blue. Scale bars are indicated on individual panels. Representative of n=3 mice. **(B)** Representative gating strategy from a Flt3:Cre, Rosa26:mTmG GEMM-shP53 tumor depicting TAM, granulocyte (Gran) and monocyte (Mono) identification in brain tumors. Bulk myeloid cells were first identified as $Cd45^{+}Cd11b^{+}$ and further subdivided into $Ly6C^{-}Ly6G^{-}$ TAM, $Ly6C^{low}Ly6G^{+}$ granulocytes, or $Ly6C^{+}Ly6G^{-}$ monocytes. **(C)** TAMs, as described in (B), from a Flt3:Cre Rosa26:mTmG GL261 tumor depicting both $TdTomato^{+}GFP^{-}$ microglia and $TdTomato^{-}GFP^{+}$ BMDM. Representative of n=3 mice. **(D)** Quantitation of $TdTomato^{+}$ and GFP^{+} monocytes, granulocytes and TAMs in GL261 tumors as depicted in (B,C) (left) or donor-GFP^{+} vs host-GFP^{-} TAMs from GL261 tumors in an irradiation-bone marrow transplantation lineage tracing model (right). Student's t-test $p \leq 0.02$. Bars represent mean and s.e.m. n=3-5 for each group. **(E)** Flow plots of TdTomato and eYFP expression in normal microglia (top) and blood monocytes (bottom) either 3 days (left) or 21 days (right) following tamoxifen treatment. Representative of n=4 mice. **(F)** Histogram of TdTomato (left) and eYFP (right) expression in tumor monocytes, TAM BMDM or TAM MG in the Cx3cr1:CreER-IRES-YFP; Rosa26:lslTdTomato; GL261 tumor model. Representative of n=6 mice. **(G)** Barplots of normalized RNA-seq counts for the *Ly6c2, Aif1, Mertk, Cx3cr1, P2ry12,* and *Tmem119* genes in the indicated cell populations. Bars represent mean ± s.e.m. **(H)** Differentially expressed genes between monocytes and the four TAM populations were identified (log2 fold change > ±1 and FDR<1%). Barchart depicts the number of differentially expressed genes that are shared between the different groups as in Figure 1I.

Bowman et al, Figure S2

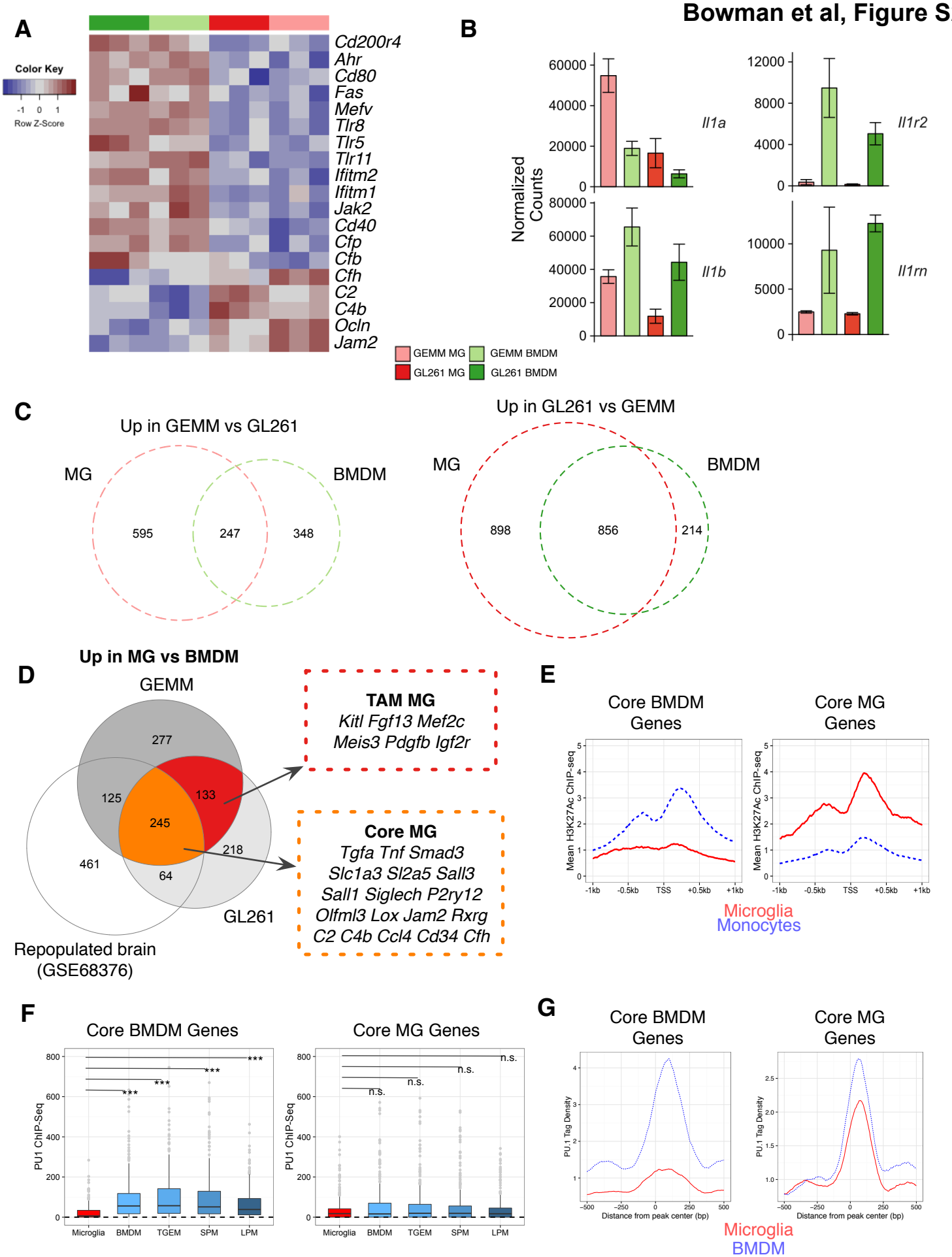

Supplemental Figure 2: TAM BMDM and TAM MG possess model and cell type specific gene expression patterns associated with baseline chromatin states. Related to Figure 2.

(A) Heatmap of row normalized gene expression values for the indicated genes across TAM BMDM and TAM MG from the GL261 and GEMM-shP53 models. **(B)** Barplots of normalized RNA-seq counts for *Il1a*, *Il1b*, *Il1r2* and *Il1rn.* Bars represent mean ± s.e.m. **(C)** Venn diagram of genes upregulated in TAM MG or TAM BMDM or both in the GEMM-shP53 model compared to the GL261 model (left). The right panel references genes that are upregulated in the GL261 model compared to the GEMM-shP53 model. **(D)** Venn diagram depicting significantly upregulated genes in MG vs BMDM in the GEMM-shP53 model, GL261 model, and non-malignant brain (GSE68376 dataset). The red sector (TAM MG genes) indicates genes that are enriched in TAM MG in both GEMM-shP53 and GL261 tumors, but are not differentially expressed in non-malignant brain. The orange sector (Core MG genes) highlights genes that are enriched in all three datasets. Select genes are listed. **(E)** Mean H3K27-Acetylation signal centered around the transcription start site (+/- 1 kb) in Core BMDM genes (left) and Core MG genes (right). Monocytes are shown in blue and microglia are shown in red. Data was downloaded and analyzed from GEO accession number GSE63339. **(F)** PU.1 binding intensity at the promoters of microglia, BMDM, thyoglycolate elicited peritoneal macrophages (TGEM), small peritoneal macrophages (SPM), and large peritoneal macrophages (LPM) for Core BMDM and Core MG genes. Genes were subset for those that showed binding of PU.1 in at least one of the macrophage populations. For Core BMDM genes with microglia vs BMDM $p \leq 7.6 \times 10^{-16}$; vs TGEM $p \leq 7.4 \times 10^{-29}$; vs SPM $p \leq 4.3 \times 10^{-29}$; vs LPM $p \leq 3.4 \times 10^{-14}$. **(G)** Mean PU.1 binding distribution in enhancers of Core BMDM and Core MG genes for microglia (red) and BMDM (blue). Enhancers were defined +/- 50 kb from the transcription start site (excluding the promoter). Data for (F) and (G) was downloaded and analyzed from GEO accession number GSE62826. n.s. denotes $p > 0.05$, *** denotes $p \leq 1 \times 10^{-13}$ evaluated with paired Student's t-test.

Bowman et al, Figure S3

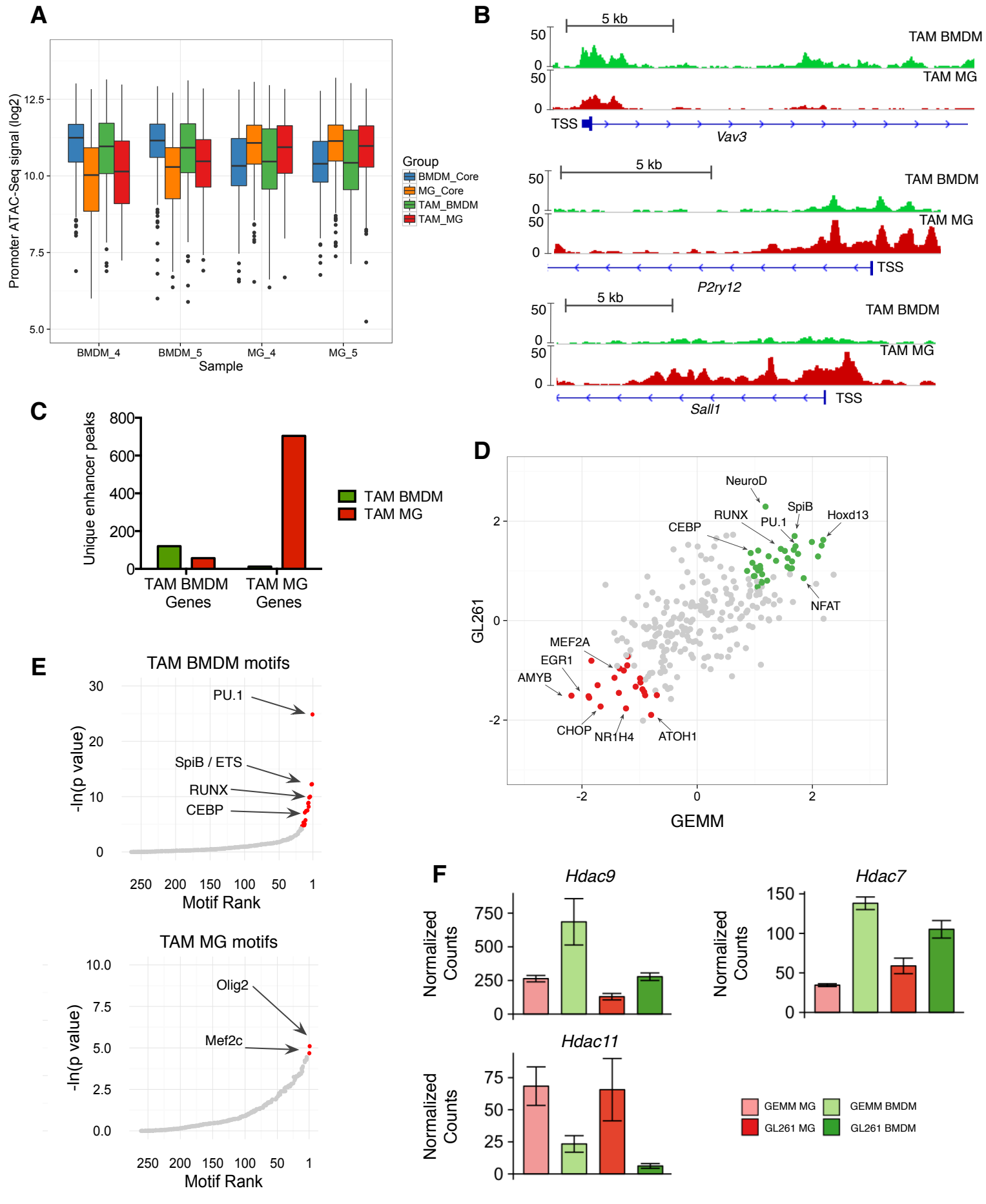

Supplemental Figure 3: TAM BMDM and TAM MG possess differential open chromatin in cell-type specific genes. Related to Figure 3.

(A) Boxplots for two matched TAM BMDM and TAM MG biological replicates of tag normalized log2 ATAC-Seq signal in the promoters of genes from the indicated gene sets, where each data point represents a score from a single promoter. **(B)** ATAC-Seq signal tracks for TAM BMDM (top, green) and TAM MG (bottom, red) around the transcription start site of *Vav3, P2ry12,* and *Sall1*. Y-axis value indicate tags per 10,000,000 with a range of 0-50. TSS denotes transcription start site. **(C)** Barplot depicting number of ATAC-seq peaks significantly enriched in either TAM BMDM or TAM MG in the indicated gene sets. **(D)** Scatterplot depicting differential transcription factor activity values between TAM BMDM and TAM MG in the GEMM-shP53 model (x-axis) and GL261 model (y-axis). Color scale and size of dot indicates relative enrichment for BMDM or MG specificity with green showing BMDM specificity and red showing MG specificity. **(E)** Ranked motifs based on –ln(p value) from HOMER for enrichment in either TAM BMDM (top) or TAM MG (bottom) genes. **(F)** Barplot depicting normalized gene counts of *Hdac7, Hdac9,* and *Hdac11* in the indicated TAM populations. Bars represent mean ± s.e.m.

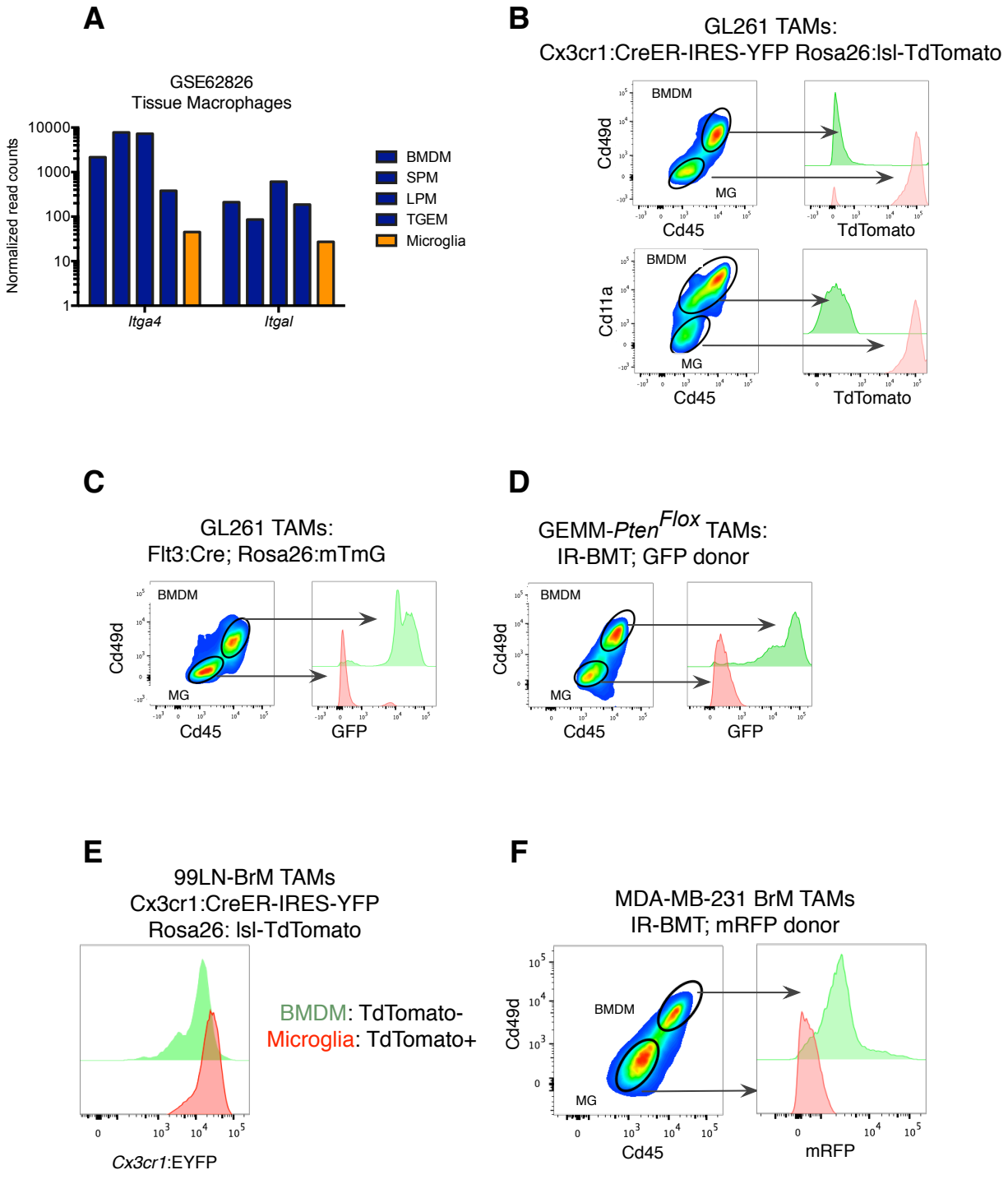
A
GSE62826
Tissue Macrophages
Normalized read counts
10000
1000
100
10
1
Itga4
Itgal
BMDM
SPM
LPM
TGEM
Microglia
B
GL261 TAMs:
Cx3cr1:CreER-IRES-YFP Rosa26:lsl-TdTomato
BMDM
MG
Cd49d
Cd45
TdTomato
Cd11a
C
GL261 TAMs:
Flt3:Cre; Rosa26:mTmG
GFP
D
GEMM-PtenFlox TAMs:
IR-BMT; GFP donor
E
99LN-BrM TAMs
Cx3cr1:CreER-IRES-YFP
Rosa26: lsl-TdTomato
Cx3cr1:EYFP
BMDM: TdTomato-
Microglia: TdTomato+
F
MDA-MB-231 BrM TAMs
IR-BMT; mRFP donor
mRFP

Supplemental Figure 4: Cd49d and Cd11a are enriched in TAM BMDM compared to TAM MG in multiple mouse models of brain malignancy. Related to Figure 4.

(A) Barchart indicating normalized gene read counts from GSE62826 for *Itga4* and *Itgal* in BMDM, small peritoneal macrophages (SPM), large peritoneal macrophages (LPM), thyoglycolate elicited peritoneal macrophages (TGEM), and microglia. Log10 y-axis as indicated. **(B)** Flow cytometry for Cd45 and either Cd49d (top) or Cd11a (bottom) on TAMs isolated from GL261 tumors in Cx3cr1:CreER-IRES-YFP Rosa26:lslTdTomato mice. The adjacent histogram depicts TdTomato expression in the indicated populations. **(C)** As in (B), but for the Flt3:Cre Rosa26:mTmG GL261 model. **(D)** Flow cytometry for Cd45 and Cd49d on TAMs isolated from a $Pten^{flox}$-GEMM tumor in a mouse that underwent IR-BMT reconstituted with GFP^+ donor cells. The adjacent histogram shows GFP expression in the indicated populations. **(E)** Histogram of eYFP expression in $TdTomato^-$ BMDM and $TdTomato^+$ MG from 99LN-BrM brain metastasis in the Cx3cr1:CreER-IRES-YFP Rosa26:lslTdTomato lineage tracing model. **(F)** Flow cytometry and associated histogram for Cd45 and Cd49d on TAMs isolated from a representative MDA-MD-231 xenograft brain metastasis in a IR-BMT mouse reconstituted with mRFP donor cells. The adjacent histogram depicts mRFP expression in the indicated populations. All flow plots are representative of n=5-8 mice.

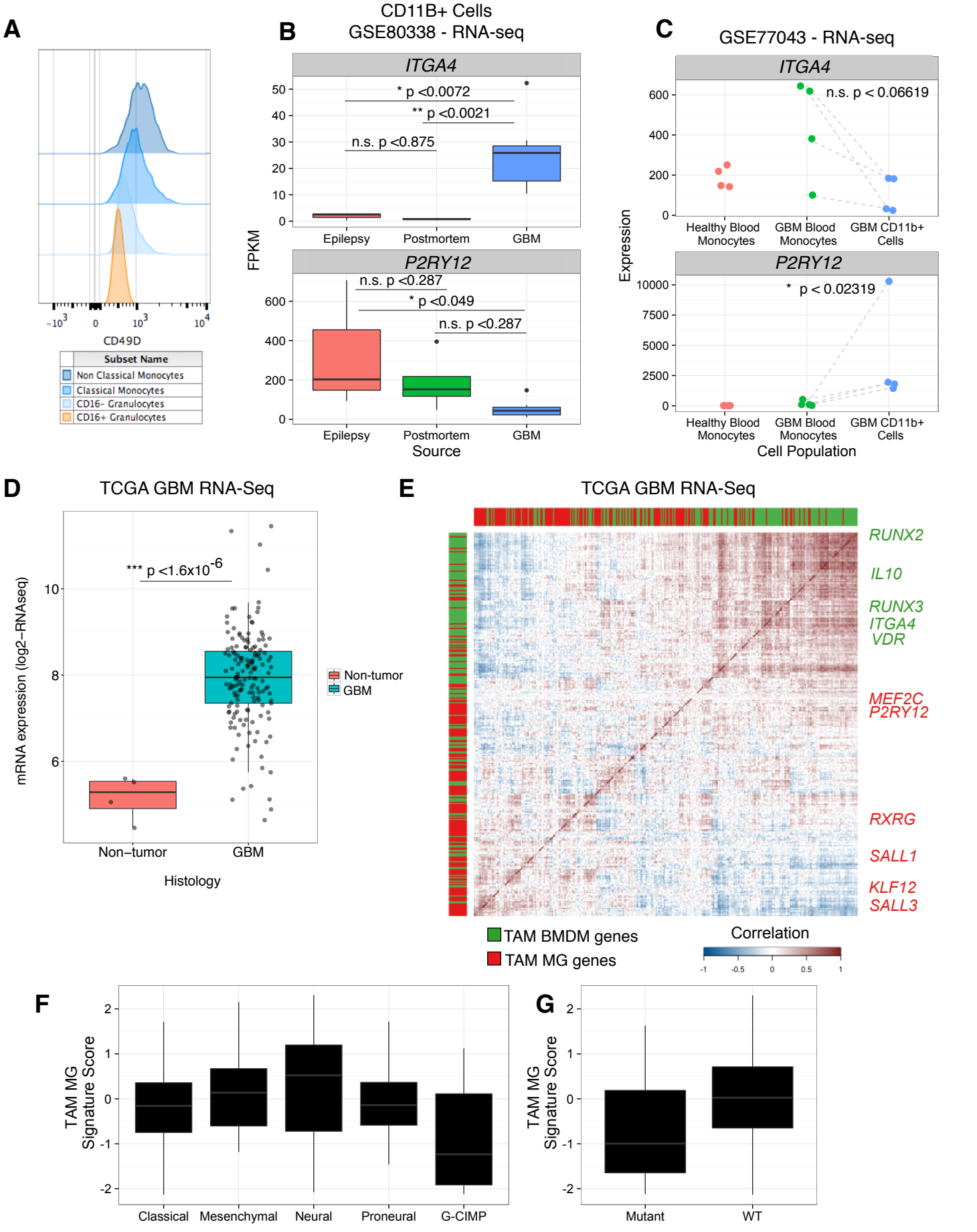
A
CD49D
Subset Name
Non Classical Monocytes
Classical Monocytes
CD16- Granulocytes
CD16+ Granulocytes
B
CD11B+ Cells
GSE80338 - RNA-seq
ITGA4
* p <0.0072
** p <0.0021
n.s. p <0.875
P2RY12
n.s. p <0.287
* p <0.049
n.s. p <0.287
FPKM
Epilepsy
Postmortem
GBM
Source
C
GSE77043 - RNA-seq
ITGA4
n.s. p < 0.06619
P2RY12
* p < 0.02319
Expression
Healthy Blood Monocytes
GBM Blood Monocytes
GBM CD11b+ Cells
Cell Population
D
TCGA GBM RNA-Seq
*** p <1.6x10-6
mRNA expression (log2-RNAseq)
Non-tumor
GBM
Histology
E
TCGA GBM RNA-Seq
RUNX2
IL10
RUNX3
ITGA4
VDR
MEF2C
P2RY12
RXRG
SALL1
KLF12
SALL3
TAM BMDM genes
TAM MG genes
Correlation
F
TAM MG Signature Score
Classical
Mesenchymal
Neural
Proneural
G-CIMP
G
TAM MG Signature Score
Mutant
WT

Supplemental Figure 5: *ITGA4* and markers of TAM BMDM are present in purified cell types and in whole tumor expression data from patients. Related to Figure 5.

(A) Histogram of CD49D expression in non-classical monocytes ($CD45^+CD11B^+CD66B^-CD16^+CD14^{low}$), classical monocytes ($CD45^+CD11B^+CD66B^-CD16^-CD14^+$), $CD16^-$ granulocytes ($CD45^+CD11B^+CD66B^+CD16^-CD14^{low}$) and $CD16^+$ granulocytes ($CD45^+CD11B^+CD66B^+CD16^+CD14^{low}$) from human healthy donor blood. Representative of n=6 samples. **(B)** Boxplot of FPKM (Fragments Per Kilobase of transcript per Million mapped reads) values from GSE80338 dataset for *ITGA4* (top) and *P2RY12* (bottom) across the indicated sample sets. (Student's t-test). **(C)** Stripchart of normalized array intensities from GSE77043 dataset for *ITGA4* (top) and *P2RY12* (bottom) across the indicated sample sets. Dashed lines indicate matched samples. (Student's t-test). **(D)** Normalized log2 RNAseq counts from TCGA-GBM dataset for *ITGA4* in non-malignant brain and GBM tissue. (Student's t-test). **(E)** Pairwise correlation matrix of TAM BMDM (green column marks) and TAM MG (red column marks) genes from the TCGA-GBM RNA-seq dataset. Blue indicates negative correlation between gene pairs and red indicates positive correlation. **(F-G)** Z-scored TAM MG signature scores across (F) tumor subtype (ANOVA $p \leq 0.041$), and (G) *IDH1* mutation status (Student's t-test $p \leq 0.153$). n.s. denotes non-significant p value, * $p \leq 0.05$, ** $p \leq 0.005$, *** $p \leq 0.0005$.

SUPPLEMENTAL EXPERIMENTAL PROCEDURES

Mouse models and cell lines

Mice

Flk2-switch (*Flt3*:Cre, Rosa26:mTmG) mice were kindly provided by Dr. Camilla Forsberg (UCSC) (Benz et al., 2008; Boyer et al., 2011; Muzumdar et al., 2007). Only male mice showed expression or transmittance of Cre, and as such only male mice could be used for these experiments. *Cx3cr1*:CreER-IRES-YFP mice were obtained from Jackson Labs and bred to Rosa26:lsl-TdTomato reporter mice (Jackson Labs) (Madisen et al., 2010; Parkhurst et al., 2013). Nestin:Tva (nTva) mice in a mixed background, as described previously, were bred to C57BL/6 background for 10 generations (Holland et al., 1998; Quail et al., 2016). *Pten*$^{Flox/Flox}$ mice (C57BL/6 background) were obtained from Dr. Charles Sawyers and Dr. Brett Carver (MSKCC) (Trotman et al., 2003). CAG:GFP mice (Okabe et al., 1997) were obtained from Jackson labs. Athymic nude mice were obtained from NCI Frederick and maintained at MSKCC. CAG:RFP mice (Long et al., 2005) were obtained from Jackson labs and crossed to Athymic nude mice for 10 generations. All animal procedures and studies were approved by the MSKCC Institutional Animal Care and Use Committee (protocol 04-08-022).

Brain tumor models

For the glioma models, intracranial injections were performed on 5-6 week old mice as previously described (Pyonteck et al., 2013). Briefly, mice were fully anesthetized with

ketamine/xylazine and bupivacaine was applied as a local anesthetic. Using a stereotactic apparatus, cells were injected into the right frontal cortex (1 mm caudal, 1.5 mm lateral from bregma, 2-3 mm deep). For the GEMM-shP53 model, $3x10^5$ DF1 cells (1:1 mixture of DF1: RCAS-PDGFB-HA, and DF1:RCAS:shP53) were injected at 6 weeks of age. For the GEMM-$Pten^{flox}$ model, $3x10^5$ cells were injected (1:1 mixture of DF1:RCAS-PDGFB-HA and DF1:RCAS-Cre) at 8 weeks of age, 4 weeks after bone marrow transplantation. For the GL261 model, $2x10^4$ cells were injected at 6 weeks of age, or 8 weeks of age if in the *Cx3cr1*:CreER-IRES-YFP lineage tracing background, 3 weeks after tamoxifen administration.

For brain metastasis models, 6-8 week old athymic nude mice or C57BL/6 mice were intracardially injected with $1x10^4$ MDA-BrM cells or 99LN-BrM cells respectively, as previously described (Bos et al., 2009; Sevenich et al., 2014). For the 99LN-BrM model in the *Cx3cr1*:CreER-IRES-YFP lineage tracing background, mice were injected with tamoxifen at 4 weeks of age, and then intracardially injected 3 weeks later, at 7 weeks of age.

Cells

DF1 chicken fibroblasts were obtained from the ATCC. RCAS vectors expressing PDGFB-HA, Cre or a short hairpin against mouse *p53* (shP53) were kindly provided by Dr. Tatsuya Ozawa and Dr. Eric Holland (Ozawa et al., 2014). GL261 murine glioma cells were kindly provided by Dr. Sal Coniglio and Dr. Jeff Segall (Albert Einstein). MDA-MB-231 brain-homing variant cells (MDA-BrM) were kindly provided by Dr. Joan Massague (MSKCC) and labeled with a triple imaging vector (Tk-GFP-Luc) as

previously described (Bos et al., 2009; Ponomarev et al., 2004; Sevenich et al., 2014). 99LN cells were derived from a metastatic lesion in the lymph node of the MMTV:PyMT genetically engineered breast cancer model (C57BL/6 background). Cells were screened *in vitro* for their invasive capacity in a transwell assay, passaged once *in vivo* in a C57BL/6 mouse and selected *in vivo* for their brain homing capacity as described previously for the MDA-MB-231 BrM variant (Bos et al., 2009). All cell lines were maintained in DMEM with 10% fetal bovine serum with penicillin and streptomycin.

Tamoxifen lineage tracing and bone marrow transplantation

For the Cx3cr1:CreER-IRES-YFP Rosa26:lsl-TdTomato lineage tracing system, 4 week-old mice were injected twice, 48 hours apart, i.p. with 1 mg of tamoxifen citrate dissolved in corn oil. Mice were used for intracranial injection of DF1 cells 3 weeks after tamoxifen administration. For bone marrow transplantation, recipient mice were irradiated (Gammacell-40 Exator) with a split dose scheme of 2x4.5 Gy with a window of 4 hours between doses. Whole bone marrow was isolated from the femurs of a CAG:GFP donor mouse (6-8 weeks old) and $1x10^6$ cells were injected i.v. into previously irradiated recipients. Athymic nude mice were irradiated with a split dosage scheme of 2x4 Gy, and were reconstituted using Athymic CAG:RFP donor cells. Experimental mice were intracranially injected with DF1 cells or intracardially injected with MDA-BrM cells 4 weeks after bone marrow transplantation.

Flow cytometry and immunohistochemistry

All antibodies for flow cytometry were titrated in a lot-dependent manner and used as follows: anti-mouse Cd45 (Biolegend 103128), anti-mouse/human Cd11b (BD Biosciences 563553), anti-mouse Ly6C (Biolegend 128026), anti-mouse Ly6G (BD Biosciences 563005), anti-mouse Cd49d (Biolegend 103618), anti-mouse Cd11a (Biolegend 101120), anti-human CD45 (Biolegend 304042), anti-human CD66B (Biolegend 305106), anti-human CD14 (Biolegend 325610), anti-human CD16 (Biolegend 302026), and anti-human CD49D (Biolegend 304308).

For tissue collection for histology, mice were anesthetized with 1.25% Avertin, and transcardially perfused with PBS and 4% paraformaldehyde (PFA). Tissues were macrodissected and the brain was post fixed in 4% PFA overnight and then placed in sucrose, while the spleen was immediately placed in 30% sucrose. Tissue was transferred to 30% sucrose for 2 days, embedded in OCT, and 10 μM cryosections were cut. Immunofluorescence staining followed. First, slides were rehydrated with two washes of PBS for 5 minutes. Tissue was then permeabilized with 0.2% Triton-X in PBS and washed twice with PBS for 5 minutes. Hydrophobic circles were drawn around tissue sections, followed by 2 more washes with PBS for 5 minutes. Tissue was blocked with 0.5% PNB blocking buffer. Primary antibody was applied in 0.25% PNB blocking buffer overnight at 4 degrees Celsius. Tissues were washed 3 times with PBS for 5 minutes. Secondary antibody was applied (1:500, Molecular Probes) for 1 hour at room temperature followed by 3 washes of PBS for 5 minutes. Slides were counterstained with DAPI (1:5000, Molecular Probes) for 5 minutes at room

temperature, washed 3 times with PBS, and mounted with Dako fluorescent mounting media. Primary antibodies used were: chicken-anti GFP (AbCam 13970, 1:500), rat anti-Cd68 (Serotec MCA1957, 1:500), and rabbit anti-Iba1 (Wako, 01-1974, 1:500). Endogenous TdTomato was visible without immunofluorescence staining from both the Rosa26:mTmG and Rosa26:lsl-TdTomato reporter mice. When combined with Cd68 staining (Figure 1J, Figure 2D), the TdTomato signal was assessed using a filter set centered around 546nm, with negligible signal present in the 594nm filter set used to collect the Cd68 signal. Images were obtained on a Zeiss Z1 AxioImager equipped with a TissueGnostics stage. Tiling images were acquired at 20x magnification using TissueFAXS (Tissuegnostics). Single images at 20x and 40x were either acquired using Axiovision (Zeiss), or extracted as single images from the TissueFAXS tiling image acquisition application (for representative images shown in Figure 1C, 1F, 1J, 2D and 4D).

External dataset download and analysis

All TCGA data was analyzed using the web-portal Gliovis (http://gliovis.bioinfo.cnio.es). Normalized gene expression data for the Immunological Genome Project (ImmGen) was obtained from the GEO under accession GSE15907 (Gautier et al., 2012). RNA-seq, ATAC-Seq and ChIP-Seq datasets for tissue resident macrophage transcriptional and epigenetic profiling were downloaded from the SRA using the NCBI SRA-toolkit from the following GEO accession numbers: GSE62826, GSE63338, and GSE63339 (Gosselin et al., 2014; Lavin et al., 2014). RNA-sequencing data on microglia and peripherally-derived macrophages in the non-malignant brain were downloaded under

accession number GSE68376 (Bruttger et al., 2015). Each of these datasets was mapped to the mouse genome mm10 as described above. For ChIP-seq and ATAC-seq datasets the STAR parameter "--alignIntronMax" was set to 1. PU.1 ChIP-Seq peak calling was performed with HOMER (Heinz et al., 2010). Peaks were considered within a promoter if they fell within 2kb upstream or 0.5kb downstream of the nearest transcription start site. Enhancer regions were considered up to 50kb upstream and downstream of the nearest transcription start site, excluding the promoter region. Deeptools was used to assess ChIP-seq and ATAC-seq density over the indicated windows surrounding either transcription start sites, or PU.1 binding sites within enhancers (Ramirez et al., 2014). The findPeaks script with HOMER was used to identify peaks for PU.1 binding with default parameters. The annotatePeaks.pl scripts in the HOMER suite was used to find enriched motifs in ChIP-seq peaks and in gene sets identified through RNA-sequencing. For promoter motif enrichment, only known motifs were considered in regions 300bp upstream and 50bp downstream of the transcription start site.

Transcription factor activity analysis:

Transcription factor (TF) activity analysis was performed as an adaptation of two previously published methods: RegulatorInference (Setty et al., 2012) and ISMARA (Balwierz et al., 2014). Briefly, a set of transcription factor binding sites (TFBS) was screened across the promoters (500bp upstream and 50bp downstream of the transcription start site) of each gene present in the mouse genome (mm10). TFBS were predicted from known motifs provided by HOMER. The AnnotatePeaks.pl script in

HOMER was used to make presence and absence calls for each TFBS in each promoter region. This was then tabulated into a matrix with TFBS motifs as columns and genes as rows. This tabulated matrix was used in a ridge regression to model log2 gene expression values generated by 'varianceStabilizingTransformation' function in the DESeq2 package in R. The glmnet function in R was used to perform the ridge regression. Lambda, the regularization parameter, was determined for each sample by 10-fold cross validation (Friedman et al., 2010). The model coefficients for each TFBS motif were z-scored. Differentially enriched TFBS motifs were determined by evaluating the z-scored values in limma with a fold change cutoff of +/-2 and a false discovery rate of 5% (Ritchie et al., 2015).

Statistical analysis and graph generation:

All statistical analyses were completed using R (version 3.0.1), GraphPad Prism Pro v6, Gliovis (http://gliovis.bioinfo.cnio.es/) or as indicated in the bioinformatics section of the methods. Heatmaps were drawn with the ggplot2, gplots (Warnes et al., 2015) packages in R. Flow cytometry biplots and histograms were plotted in FlowJo v10.8. ATAC-sequencing tracks were visualized in IGV v2.3.66. Venn diagrams were drawn with the VennDiagram (Chen, 2015) and Vennerable (Swinton) packages in R. All other scatterplots, barplots, and boxplots were plotted with the ggplot2 package in R or with GraphPad Prism Pro v6. All boxplots are depicted as Tukey-boxplots with median values, boxes indicating 25% and 75%, and whiskers extending to 1.5 times the interquartile range. All code used in this study can be found at the following website: https://bitbucket.org/bowmanr/joycelab-brain-tme.

SUPPLEMENTAL REFERENCES

Balwierz, P.J., Pachkov, M., Arnold, P., Gruber, A.J., Zavolan, M., and van Nimwegen, E. (2014). ISMARA: automated modeling of genomic signals as a democracy of regulatory motifs. *Genome Research* 24, 869-884.

Benz, C., Martins, V.C., Radtke, F., and Bleul, C.C. (2008). The stream of precursors that colonizes the thymus proceeds selectively through the early T lineage precursor stage of T cell development. *The Journal of Experimental Medicine* 205, 1187-1199.

Bos, P.D., Zhang, X.H., Nadal, C., Shu, W., Gomis, R.R., Nguyen, D.X., Minn, A.J., van de Vijver, M.J., Gerald, W.L., Foekens, J.A., and Massague, J. (2009). Genes that mediate breast cancer metastasis to the brain. *Nature* 459, 1005-1009.

Boyer, S.W., Schroeder, A.V., Smith-Berdan, S., and Forsberg, E.C. (2011). All hematopoietic cells develop from hematopoietic stem cells through Flk2/Flt3-positive progenitor cells. *Cell Stem Cell* 9, 64-73.

Bruttger, J., Karram, K., Wortge, S., Regen, T., Marini, F., Hoppmann, N., Klein, M., Blank, T., Yona, S., Wolf, Y., et al. (2015). Genetic cell ablation reveals clusters of local self-renewing microglia in the mammalian central nervous system. *Immunity* 43, 92-106.

Chen, H. (2015). VennDiagram: generate high-resolution Venn and Euler plots.

Friedman, J., Hastie, T., and Tibshirani, R. (2010). Regularization paths for generalized linear models via coordinate descent. *Journal of Statistical Software* 33, 1-22.

Gautier, E.L., Shay, T., Miller, J., Greter, M., Jakubzick, C., Ivanov, S., Helft, J., Chow, A., Elpek, K.G., Gordonov, S., et al. (2012). Gene-expression profiles and transcriptional regulatory pathways that underlie the identity and diversity of mouse tissue macrophages. *Nature Immunology* 13, 1118-1128.

Gosselin, D., Link, V.M., Romanoski, C.E., Fonseca, G.J., Eichenfield, D.Z., Spann, N.J., Stender, J.D., Chun, H.B., Garner, H., Geissmann, F., and Glass, C.K. (2014). Environment drives selection and function of enhancers controlling tissue-specific macrophage identities. *Cell* 159, 1327-1340.

Heinz, S., Benner, C., Spann, N., Bertolino, E., Lin, Y.C., Laslo, P., Cheng, J.X., Murre, C., Singh, H., and Glass, C.K. (2010). Simple combinations of lineage-determining transcription factors prime cis-regulatory elements required for macrophage and B cell identities. *Molecular Cell* 38, 576-589.

Holland, E.C., Hively, W.P., DePinho, R.A., and Varmus, H.E. (1998). A constitutively active epidermal growth factor receptor cooperates with disruption of G1 cell-cycle arrest pathways to induce glioma-like lesions in mice. *Genes & Development* 12, 3675-3685.

Lavin, Y., Winter, D., Blecher-Gonen, R., David, E., Keren-Shaul, H., Merad, M., Jung, S., and Amit, I. (2014). Tissue-resident macrophage enhancer landscapes are shaped by the local microenvironment. *Cell* 159, 1312-1326.

Long, J.Z., Lackan, C.S., and Hadjantonakis, A.K. (2005). Genetic and spectrally distinct in vivo imaging: embryonic stem cells and mice with widespread expression of a monomeric red fluorescent protein. *BMC Biotechnology* 5, 20.

Madisen, L., Zwingman, T.A., Sunkin, S.M., Oh, S.W., Zariwala, H.A., Gu, H., Ng, L.L., Palmiter, R.D., Hawrylycz, M.J., Jones, A.R., et al. (2010). A robust and high-throughput Cre reporting and characterization system for the whole mouse brain. *Nature Neuroscience* 13, 133-140.

Muzumdar, M.D., Tasic, B., Miyamichi, K., Li, L., and Luo, L. (2007). A global double-fluorescent Cre reporter mouse. *Genesis* 45, 593-605.

Okabe, M., Ikawa, M., Kominami, K., Nakanishi, T., and Nishimune, Y. (1997). 'Green mice' as a source of ubiquitous green cells. *FEBS Letters* 407, 313-319.

Ozawa, T., Riester, M., Cheng, Y.K., Huse, J.T., Squatrito, M., Helmy, K., Charles, N., Michor, F., and Holland, E.C. (2014). Most human non-GCIMP glioblastoma subtypes evolve from a common proneural-like precursor glioma. *Cancer Cell* 26, 288-300.

Parkhurst, C.N., Yang, G., Ninan, I., Savas, J.N., Yates, J.R., 3rd, Lafaille, J.J., Hempstead, B.L., Littman, D.R., and Gan, W.B. (2013). Microglia promote learning-dependent synapse formation through brain-derived neurotrophic factor. *Cell* 155, 1596-1609.

Ponomarev, V., Doubrovin, M., Serganova, I., Vider, J., Shavrin, A., Beresten, T., Ivanova, A., Ageyeva, L., Tourkova, V., Balatoni, J., et al. (2004). A novel triple-modality reporter gene for whole-body fluorescent, bioluminescent, and nuclear noninvasive imaging. *European Journal of Nuclear Medicine and Molecular Imaging* 31, 740-751.

Pyonteck, S.M., Akkari, L., Schuhmacher, A.J., Bowman, R.L., Sevenich, L., Quail, D.F., Olson, O.C., Quick, M.L., Huse, J.T., Teijeiro, V., et al. (2013). CSF-1R inhibition alters macrophage polarization and blocks glioma progression. *Nature Medicine* 19, 1264-1272.

Quail, D.F., Bowman, R.L., Akkari, L., Quick, M.L., Schuhmacher, A.J., Huse, J.T., Holland, E.C., Sutton, J.C., and Joyce, J.A. (2016). The tumor microenvironment underlies acquired resistance to CSF-1R inhibition in gliomas. Science *352*, aad3018.

Ramirez, F., Dundar, F., Diehl, S., Gruning, B.A., and Manke, T. (2014). deepTools: a flexible platform for exploring deep-sequencing data. *Nucleic Acids Research* 42, W187-191.

Ritchie, M.E., Phipson, B., Wu, D., Hu, Y., Law, C.W., Shi, W., and Smyth, G.K. (2015). limma powers differential expression analyses for RNA-sequencing and microarray studies. *Nucleic Acids Research* 43, e47.

Setty, M., Helmy, K., Khan, A.A., Silber, J., Arvey, A., Neezen, F., Agius, P., Huse, J.T., Holland, E.C., and Leslie, C.S. (2012). Inferring transcriptional and microRNA-mediated regulatory programs in glioblastoma. *Molecular Systems Biology* 8, 605.

Sevenich, L., Bowman, R.L., Mason, S.D., Quail, D.F., Rapaport, F., Elie, B.T., Brogi, E., Brastianos, P.K., Hahn, W.C., Holsinger, L.J., et al. (2014). Analysis of tumour- and stroma-supplied proteolytic networks reveals a brain-metastasis-promoting role for cathepsin S. *Nature Cell Biology* 16, 876-888.

Swinton, J. Vennerable: Venn and Euler area-proportional diagrams.

Trotman, L.C., Niki, M., Dotan, Z.A., Koutcher, J.A., Di Cristofano, A., Xiao, A., Khoo, A.S., Roy-Burman, P., Greenberg, N.M., Van Dyke, T., et al. (2003). Pten dose dictates cancer progression in the prostate. *PLoS Biology* 1, E59.

Warnes, G.R., Bolker, B., Bonebakker, L., Gentleman, R., Huber, W., Liaw, A., Lumley, T., Maechler, M., Magnusson, A., Moeller, S., et al. (2015). gplots: Various R Programming Tools for Plotting Data.